

Movable Antenna-enabled RIS-aided Integrated Sensing and Communication

Haisu Wu, Hong Ren, *Member, IEEE*, Cunhua Pan, *Senior Member, IEEE*, Yang Zhang

Abstract—In this paper, we investigate a movable antenna (MA)-aided integrated sensing and communication (ISAC) system, where a reconfigurable intelligent surface (RIS) is employed to enhance wireless communication and sensing performance in dead zones. Specifically, this paper aims to maximize the minimum beampattern gain at the RIS by jointly optimizing the covariance matrix at the base station (BS), the reflecting coefficients at the RIS and the positions of the MAs, subject to signal-to-interference-plus-noise ratio (SINR) constraint for the users and maximum transmit power at the BS. To tackle this non-convex optimization problem, we propose an alternating optimization (AO) algorithm and employ semidefinite relaxation (SDR), sequential rank-one constraint relaxation (SRCR) and successive convex approximation (SCA) techniques. Numerical results indicate that the MA-enabled RIS-aided ISAC system outperforms conventional fixed position antenna (FPA) and RIS-aided systems. In addition, the application of MAs can reconfigure geometric properties of the antenna array and enhance channel gain in the ISAC system.

Index Terms—Movable antenna (MA), integrated sensing and communication (ISAC), reconfigurable intelligent surface (RIS), antenna position optimization.

I. INTRODUCTION

FUTURE sixth generation (6G) communication is anticipated to support applications such as Massive Internet of Things (Massive-IoT), industrial automation (IA), and virtual reality (VR), which demand higher sensing precision and lower communication latency. These demands for 6G technologies call for a paradigm shift in the existing wireless communication networks. In particular, integrated sensing and communication (ISAC) is regarded as one of the key transformative technologies for future 6G networks [1], [2]. The objective of ISAC is to consolidate the sensing and communication functions onto a unified platform which allows for the sharing of resources, hardware facilities, and signal-processing modules, thereby enhancing both spectrum and hardware efficiency. In addition, millimeter-wave (mmW)/Terahertz (THz) signals [3] and ultra-massive multiple-input multiple-output (MIMO) [4] are expected to be utilized in the future communication system, implying that future wireless communication and radar sensing systems will become similar in hardware, which further enables the sharing of hardware resources.

Based on the aforementioned background, dual-functional radar and communication (DFRC) is proposed as a paradigm

of ISAC systems, which performs both sensing and communication functions with shared frequency spectrum on an identical hardware platform [5], [6]. Compared with another framework of ISAC, namely radar and communication coexistence (RCC), the integration of DFRC can reduce hardware costs and simplify design complexity. Currently, DFRC has received increasing attention, and most of the related investigations considered the beamforming design at the DFRC base station (BS). For instance, the authors of [1] initially considered the beampattern design in a DFRC system. Specifically, the spatial beamforming waveform at the DFRC BS is optimized to minimize the power of the interference for downlink communication users, subject to several design criteria of the radar. In addition, the authors of [7] investigated the beamforming design of a co-located MIMO system with a monostatic DFRC radar. Specifically, the authors proposed the simultaneous transmission of radar waveforms and communication symbols, which can form multiple beams and better exploit the degrees of freedom (DoFs) in the MIMO system. Based on the aforementioned works, the authors of [8] considered the transmit beamforming in a downlink ISAC system to enhance the radar sensing performance while guaranteeing the user SINR constraint. In particular, the authors investigated the impact of whether the receivers could cancel the interference from dedicated radar signals on sensing performance. Nevertheless, although mmW/THz signals can provide extensive bandwidth which is capable of enhancing the communication and sensing performance, the high frequency will lead to increased susceptibility of the transmit signal to be obstructed. In scenarios where the line-of-sight (LoS) links between the DFRC BS and the targets are obstructed, the performance of the ISAC system will experience substantial degradation.

Reconfigurable intelligent surface (RIS) is considered as a promising technology to address the aforementioned challenges [9]–[11]. An RIS is a meta-surface consisting of passive reflecting elements, each of which is capable of independently altering the phases of incident signals. Therefore, the RIS can intelligently reconstruct the wireless channels, thereby strengthening the quality of service (QoS) of the legitimate users. In terms of the sensing function, RIS can also establish virtual LoS links in dead zones of the DFRC BS, significantly improving sensing capability in the ISAC systems [12]–[15]. For instance, the authors of [12] jointly optimized the transmit beamforming and the phase shifts of the RIS to maximize the minimum beampattern gain towards the desired directions in the non-line-of-sight (NLoS) area of the BS, subject to communication SINR constraint of a single user. Furthermore, the authors of [13] proposed the novel scheme of using two

H. Wu is a bachelor's degree graduate from Shandong University, Weihai, China. (e-mail: wuhaisu2020@gmail.com). He will join Southeast University as a Master student. H. Ren, C. Pan and Y. Zhang are with National Mobile Communications Research Laboratory, Southeast University, Nanjing, China. (e-mail: hren, cpan, 220230982@seu.edu.cn).

Corresponding authors: Hong Ren and Cunhua Pan.

dedicated RISs for enhancing communication and sensing tasks respectively. They also demonstrated that the sensing performance can be greatly enhanced when targets are located at the NLoS area of the BS.

Nonetheless, in the aforementioned ISAC systems, the MIMO architectures generally utilized fixed position antenna (FPA) arrays, which restrict the full utilization of the available DoFs within the continuous spatial domain, thereby hindering optimal spatial diversity and multiplexing performance in communication and sensing tasks. Furthermore, the unchangeable geometric configurations of conventional FPA arrays can lead to certain array gain loss during radar beamforming tasks.

Recently, the novel concept of movable antenna (MA) has been proposed as an innovative solution to overcome the inherent limitations in FPA systems [16]–[18]. By facilitating a driver component or similar mechanisms, the positions of MAs can be adjusted dynamically within a designated spatial area, thereby reconstructing channel conditions to boost communication performance, or reconfiguring the geometric properties of the MIMO arrays to enhance sensing capability. Channel modeling for MA-aided communication systems was explored in [18], where the authors introduced a field-response channel model. They conducted a comparative performance analysis of MA-aided and FPA systems across deterministic and statistical channels, highlighting the substantial advantages in enhancing received power and reducing outage probability of the MA-aided system. In [19], [20], the research explored channel estimation for MA-aided communication systems by using compressed sensing and deep learning method, respectively. Based on perfect channel state information (CSI), extensive research has shown that MA-aided systems provide substantial improvements over traditional FPA systems in wireless communication [21]–[25]. For example, MA-aided multi-terminal uplink transmission system with an FPA BS was investigated in [21], where a power minimization problem was formulated subject to minimum-achievable-rate of terminals, and a gradient descent-based iterative method was proposed to optimize the positions of MAs.

Nevertheless, the potential of MA in the field of wireless sensing has not yet been fully explored, and only a few existing studies considered wireless sensing without communication [26], [27]. The authors of [26] investigated the enhanced multi-beam forming with a linear MA array by optimizing antenna positions to exploit new DoFs. In addition, in [27], the authors delved into both one-dimensional (1D) and two-dimensional (2D) MA arrays and demonstrated that the MA arrays can greatly improve sensing capacity of the system over their FPA counterparts both analytically and numerically. Notably, numerical simulations revealed lower correlation of the steering vectors for 1D/2D MA arrays, which can enhance wireless sensing performance. Furthermore, the authors of [28] introduced linear 1D MA into ISAC system, and then considered relatively simple settings where the transmit beamforming at the BS and the positions of the MAs were jointly optimized to maximize the communication rate and sensing mutual information. However, these studies all considered the LoS links between the BS and the targets. In contrast, if the targets may locate in the NLoS area of the BS, it is reasonable

to apply an RIS to enhance the sensing performance of the MA-aided system.

Against the above background, this paper considers an ISAC system which is assisted by a 2D MA array and an RIS for effective wireless sensing and communication in dead zones. The main contributions of our paper are summarized as follows:

- We consider an MA and RIS-aided ISAC system, where a DFRC BS equipped with a 2D MA array aims to sense the targets located in multiple angles and serve the communication users. In particular, the angles of interest are located in the NLoS area of the DFRC BS, thus an RIS is deployed to create a virtual LoS link to enhance the wireless sensing and communication performance. Then, we formulate the minimum beampattern gain maximization problem subject to communication SINR constraints.
- To address this highly non-convex optimization problem, we propose an AO-based algorithm which incorporates several techniques: semidefinite relaxation (SDR), sequential rank-one constraint relaxation (SRCR) and successive convex approximation (SCA). Specifically, we optimize the transmit beamforming at the BS by using SDR and the phase shifts at the RIS by using the SRCR algorithm to avoid potential non-convergence issues of SDR. For the tightly coupled positions of MAs, we iteratively optimize individual antenna positions by using the SCA algorithm while fixing the positions of other antennas to obtain a suboptimal solution.
- Simulation results confirm the performance improvement of deploying MAs in RIS-aided ISAC systems compared to FPAs. In addition, the application of MAs can reduce the similarity of user channels in ISAC systems, thereby effectively mitigating multi-user interference. Furthermore, antenna displacement can alleviate multipath effects caused by channel fading and enhance channel gain.

Notations: Boldface lower case and upper case letters denote vectors and matrices, respectively. $(\cdot)^*$, $(\cdot)^T$ and $(\cdot)^H$ denote the conjugate, transpose and conjugate transpose (Hermitian), respectively. $\mathbb{E}[\cdot]$ denotes the expectation operation. $\|\mathbf{a}\|_2$ denotes the 2-norm of vector \mathbf{a} . The set of $P \times Q$ complex and real matrices is denoted by $\mathbb{C}^{P \times Q}$ and $\mathbb{R}^{P \times Q}$, respectively. We use $[\mathbf{A}]_{p,q}$ to denote the entry of matrix \mathbf{A} in its p -th row and q -th column. $\Re\{\mathbf{a}\}$ denotes the real part of vector \mathbf{a} . $\text{diag}(\mathbf{a})$ denotes a square diagonal matrix with the elements of vector \mathbf{a} as its diagonal elements, while $\text{diag}(\mathbf{A})$ denotes a column vector consisting of the main diagonal elements of matrix \mathbf{A} . $\mathbf{A} \succeq 0$ indicates that \mathbf{A} is a positive semidefinite matrix. $\mathcal{CN}(0, \sigma^2)$ denotes the circularly symmetric complex Gaussian (CSCG) distribution with zero mean and covariance σ^2 . $\text{rank}(\mathbf{A})$ denotes the rank of matrix \mathbf{A} . The amplitude and phase of complex value a are denoted by $|a|$ and $\angle a$, respectively.

II. SYSTEM MODEL AND PROBLEM FORMULATION

We consider an MA and RIS-aided ISAC system as depicted in Fig. 1, where a DFRC BS equipped with a uniform linear array (ULA) of M antennas serves K single-antenna users

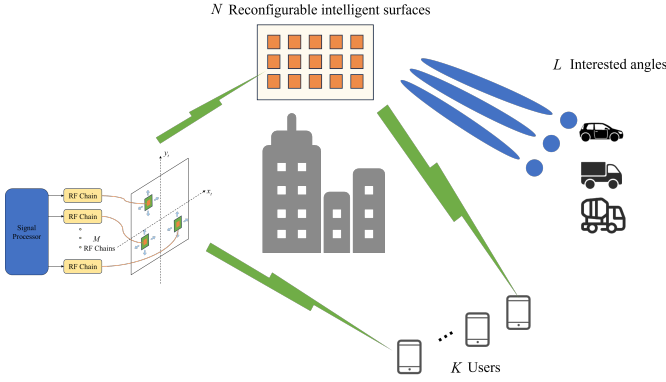


Fig. 1: MA and RIS-aided ISAC system.

and detects targets located in the NLoS area of the DFRC BS. In addition, an RIS with N reflecting elements is deployed in the system to enhance the communication and sensing performance, and it is assumed that the targets are located at L interested angles towards the RIS.

A. Signal Model

The transmit signal of the DFRC BS is represented as

$$\mathbf{x} = \mathbf{W}_r \mathbf{s} + \mathbf{W}_c \mathbf{c} = [\mathbf{W}_r, \mathbf{W}_c] [\mathbf{s}^T, \mathbf{c}^T]^T = \mathbf{W} \hat{\mathbf{x}}, \quad (1)$$

where $\mathbf{s} \in \mathbb{C}^{M \times 1}$ is the radar signal, and $\mathbf{c} \in \mathbb{C}^{K \times 1}$ denotes the transmit symbols to the K users. In addition, $\mathbf{W}_r = [\mathbf{w}_{r,1}, \mathbf{w}_{r,2}, \dots, \mathbf{w}_{r,M}] \in \mathbb{C}^{M \times M}$, $\mathbf{W}_c = [\mathbf{w}_{c,1}, \mathbf{w}_{c,2}, \dots, \mathbf{w}_{c,K}] \in \mathbb{C}^{M \times K}$ denote the beamforming matrices for radar and communication, respectively. $\mathbf{W} = [\mathbf{W}_r, \mathbf{W}_c] \in \mathbb{C}^{M \times (M+K)}$ represents the equivalent DFRC transmit beamforming matrix. It is assumed that the radar signals are generated by pseudo-random coding, which satisfies $\mathbb{E}[\mathbf{s}] = \mathbf{0}$ and $\mathbb{E}[\mathbf{s}\mathbf{s}^H] = \mathbf{I}_M$. The communication signal \mathbf{c} is assumed to follow $\mathcal{CN}(\mathbf{0}, \mathbf{I}_K)$, and the radar and communication signals are uncorrelated. Therefore, the covariance matrix of the transmit signal can be expressed as

$$\mathbf{R} = \mathbb{E}[\mathbf{x}\mathbf{x}^H] = \mathbf{W}\mathbf{W}^H = \mathbf{W}_r\mathbf{W}_r^H + \sum_{k=1}^K \mathbf{R}_k, \quad (2)$$

where the rank-one matrix \mathbf{R}_k is introduced by $\mathbf{R}_k \triangleq \mathbf{w}_{c,k}\mathbf{w}_{c,k}^H$.

B. Channel Model

This paper utilizes the planar far-field response model in [18], where each transmit/receive path of the same channel has the same angle of departure (AoD), angle of arrival (AoA), and path response coefficient, but different signal phases. Specifically, let us define $\tilde{\mathbf{t}} = [\mathbf{t}_1, \mathbf{t}_2, \dots, \mathbf{t}_M] \in \mathbb{R}^{2 \times M}$ as the positions of MAs at the BS, where $\mathbf{t}_m = [x_m, y_m]^T \in \mathcal{C}$, $1 \leq m \leq M$ represents the coordinates of the m -th MA, and \mathcal{C} is the transmit region of the MAs.

As shown in Fig. 2, the elevation and azimuth angles of the transmit area and the receive area are denoted as $\theta_j^t \in [0, \pi]$, $\phi_j^t \in [0, \pi]$, $1 \leq j \leq L_t$ and $\theta_i^r \in [0, \pi]$, $\phi_i^r \in$

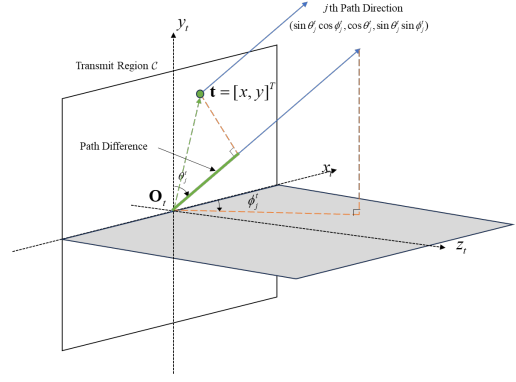


Fig. 2: Illustration of the coordinates and spatial angles in transmit region.

$[0, \pi]$, $1 \leq i \leq L_r$, respectively. Here, L_t is the number of transmit paths from the BS to the RIS, and L_r is the number of receive paths at the RIS, respectively. In addition, the number of transmit paths for the direct channel from the BS to the k -th user is defined as L_t^k , $1 \leq k \leq K$. For the MA-aided system, the channel matrix is determined by the signal propagation environment and the MAs' positions. According to [18], the field response vector (FRV) of the MA at position $\mathbf{t} = [x, y]^T$ in the BS-RIS link is given by

$$\mathbf{g}(\mathbf{t}) = \left[e^{j\frac{2\pi}{\lambda}\rho_t^1(\mathbf{t})}, e^{j\frac{2\pi}{\lambda}\rho_t^2(\mathbf{t})}, \dots, e^{j\frac{2\pi}{\lambda}\rho_t^{L_t}(\mathbf{t})} \right]^T \in \mathbb{C}^{L_t \times 1}, \quad (3)$$

where λ represents the wavelength and $\rho_t^j(\mathbf{t}) = x \sin \theta_j^t \cos \phi_j^t + y \cos \theta_j^t$ represents the difference of the signal propagation distance for the j -th transmit path between position \mathbf{t} and reference origin. Therefore, the field response matrix (FRM) of the BS-RIS link for all M transmit MAs is given by

$$\mathbf{G}(\tilde{\mathbf{t}}) \triangleq [\mathbf{g}(\mathbf{t}_1), \mathbf{g}(\mathbf{t}_2), \dots, \mathbf{g}(\mathbf{t}_M)] \in \mathbb{C}^{L_t \times M}. \quad (4)$$

Similarly, the FRM of the BS-User link for all M MAs is:

$$\mathbf{G}_k(\tilde{\mathbf{t}}) \triangleq [\mathbf{g}_k(\mathbf{t}_1), \mathbf{g}_k(\mathbf{t}_2), \dots, \mathbf{g}_k(\mathbf{t}_M)] \in \mathbb{C}^{L_t^k \times M}, 1 \leq k \leq K. \quad (5)$$

In addition, it can be derived that the FRV for a single reflecting element at the RIS is

$$\mathbf{f}(\mathbf{r}) = \left[e^{j\frac{2\pi}{\lambda}\rho_r^1(\mathbf{r})}, e^{j\frac{2\pi}{\lambda}\rho_r^2(\mathbf{r})}, \dots, e^{j\frac{2\pi}{\lambda}\rho_r^{L_r}(\mathbf{r})} \right]^T \in \mathbb{C}^{L_r \times 1}, \quad (6)$$

where $\rho_r^i(\mathbf{r}) = x \sin \theta_i^r \cos \phi_i^r + y \cos \theta_i^r$ is the difference of the signal propagation distance for the i -th receive path between the element position \mathbf{r} and the origin of the RIS. Hence, the FRM at the RIS is represented as

$$\mathbf{F}(\mathbf{r}) = [\mathbf{f}(\mathbf{r}_1), \mathbf{f}(\mathbf{r}_2), \dots, \mathbf{f}(\mathbf{r}_N)] \in \mathbb{C}^{L_r \times N}. \quad (7)$$

Then, let us denote the path response matrix (PRM) $\Sigma \in \mathbb{C}^{L_r \times L_t}$ and $\Sigma_k \in \mathbb{C}^{L_r^k \times L_t^k}$, $1 \leq k \leq K$ as the responses of all transmit and receive paths from the BS to the RIS and from the BS to the k -th user, respectively. Therefore, the channel matrix from the BS to the RIS can be expressed as

$$\mathbf{H}(\tilde{\mathbf{t}}) = \mathbf{F}(\mathbf{r})^H \Sigma \mathbf{G}(\tilde{\mathbf{t}}). \quad (8)$$

Similarly, the channel from the BS to the k -th user can be given by

$$\mathbf{h}_{1,k}^H(\tilde{\mathbf{t}}) = \mathbf{1}^H \Sigma_k \mathbf{G}_k(\tilde{\mathbf{t}}) \in \mathbb{C}^{1 \times M}. \quad (9)$$

Furthermore, the positions of RIS elements and antennas of the users are fixed, and the channel matrix from the RIS to the k -th user can be represented as $\mathbf{h}_{2,k}^H \in \mathbb{C}^{1 \times N}$. We also assume that the CSI of the channels is perfectly known at the DFRC BS with the application of MA-related channel estimation methods [19], [20].

C. Communication and Radar Sensing Metrics

By combining the signals from both BS-User and BS-RIS-User links, the received signal at the k -th user is

$$y_k = (\mathbf{h}_{2,k}^H \Phi \mathbf{H}(\tilde{\mathbf{t}}) + \mathbf{h}_{1,k}^H(\tilde{\mathbf{t}})) \mathbf{x} + n_k, \quad (10)$$

where $n_k \sim \mathcal{CN}(0, \sigma_k^2)$ denotes additive white Gaussian noise (AWGN) at the k -th user receiver. Thus, the SINR for the k -th user is

$$\begin{aligned} \text{SINR}_k &= \frac{\mathbf{h}_k^H \mathbf{w}_k \mathbf{w}_k^H \mathbf{h}_k}{\sum_{1 \leq i \leq M+K, i \neq k} \mathbf{h}_k^H \mathbf{w}_i \mathbf{w}_i^H \mathbf{h}_k + \sigma_k^2} \\ &= \frac{\mathbf{h}_k^H \mathbf{R}_k \mathbf{h}_k}{\sum_{1 \leq i \leq M+K, i \neq k} \mathbf{h}_k^H \mathbf{R}_i \mathbf{h}_k + \sigma_k^2} \\ &= \frac{\mathbf{h}_k^H \mathbf{R}_k \mathbf{h}_k}{\mathbf{h}_k^H (\mathbf{R} - \mathbf{R}_k) \mathbf{h}_k + \sigma_k^2}, \end{aligned} \quad (11)$$

where $\mathbf{h}_k^H(\tilde{\mathbf{t}}) \triangleq \mathbf{h}_{2,k}^H \Phi \mathbf{H}(\tilde{\mathbf{t}}) + \mathbf{h}_{1,k}^H(\tilde{\mathbf{t}})$ represents the equivalent channel between the BS and the k -th user.

Next, we consider the perception of potential targets in the NLoS area of BS. In this case, we assume that the virtual LoS channel created by the RIS are much stronger than the NLoS one. Hence, the effect of NLoS channel between the BS and sensing targets can be neglected. In addition, it is assumed that the location of the RIS is well designed with few obstacles, and we adopt the beam direction gain of the RIS at the desired sensing angles as the sensing performance metrics. Let d_{RIS} represent the spacing between consecutive reflecting elements at the RIS, and the steering vector at the RIS is given by

$$\mathbf{a}(\theta) = \left[1, e^{j \frac{2\pi d_{\text{RIS}}}{\lambda} \sin \theta}, \dots, e^{j \frac{2\pi (N-1) d_{\text{RIS}}}{\lambda} \sin \theta} \right]^T, \quad (12)$$

where θ denotes the AoD of the target towards the RIS. We also consider that both the signal symbol \mathbf{c} and the radar symbol \mathbf{s} can be used for sensing [7]. Therefore, the beampattern gain at the RIS corresponding to angle θ is

$$\begin{aligned} \mathcal{P}(\theta) &= \mathbb{E} \left(\left| \mathbf{a}(\theta)^H \Phi \mathbf{H}(\tilde{\mathbf{t}}) (\mathbf{W}_{r,s} + \mathbf{W}_{c,c}) \right|^2 \right) \\ &= \mathbf{a}(\theta)^H \Phi \mathbf{H}(\tilde{\mathbf{t}}) \mathbf{R} \mathbf{H}(\tilde{\mathbf{t}})^H \Phi^H \mathbf{a}(\theta). \end{aligned} \quad (13)$$

We are interested in L specific angles $\{\theta_1, \dots, \theta_L\}$, and we define $\mathcal{L} \triangleq \{1, \dots, L\}$ as the set of sensing angles of interest.

D. Problem Formulation

In this paper, we aim to maximize the minimum beampattern gain in the directions of the L interested sensing angles by jointly optimizing the covariance matrix \mathbf{R} of the transmit beamformer at the BS, the phase shifts Φ at the RIS, and the positions $\tilde{\mathbf{t}}$ of the MAs. Accordingly, the problem is formulated as

$$\max_{\mathbf{R}, \Phi, \tilde{\mathbf{t}}} \min_{l \in \mathcal{L}} \mathbf{a}(\theta_l)^H \Phi \mathbf{H}(\tilde{\mathbf{t}}) \mathbf{R} \mathbf{H}(\tilde{\mathbf{t}})^H \Phi^H \mathbf{a}(\theta_l) \quad (14a)$$

$$\text{s.t.} \quad \text{SINR}_k \geq \Gamma, \forall k, \quad (14b)$$

$$\text{tr}(\mathbf{R}) \leq P_0, \quad (14c)$$

$$\mathbf{R} \succeq 0, \quad (14d)$$

$$\text{rank}(\mathbf{R}_k) = 1 \quad (14e)$$

$$\Phi = \text{diag}(e^{j\phi_1}, \dots, e^{j\phi_N}), \quad (14f)$$

$$\|\mathbf{t}_k - \mathbf{t}_q\|_2 \geq D, \quad k \neq q, \quad (14g)$$

$$\tilde{\mathbf{t}} \in \mathcal{C}, \quad (14h)$$

where P_0 denotes the maximum transmit power at the BS, Γ denotes the minimum SINR threshold of the users, and D represents the minimum distance between MAs to prevent coupling effects.

It is challenging to solve Problem (14) due to the intricately coupled variables \mathbf{R} , Φ , $\tilde{\mathbf{t}}$. Furthermore, the objective function of Problem (14) exhibits non-smooth characteristics, and the channel vectors are highly non-convex with respect to MA positions $\tilde{\mathbf{t}}$, which increases the difficulty of solving Problem (14).

III. PROPOSED AO-BASED ALGORITHM

In this section, we decouple the original problem into three subproblems and optimize them alternately. Specifically, we employ the SDR algorithm to optimize the transmit covariance matrix \mathbf{R} , and utilize the SRCR algorithm to optimize the reflecting coefficient Φ . Subsequently, the positions of MAs, denoted as $\tilde{\mathbf{t}}$, are optimized by using the SCA technique.

A. Transmit Beamforming Optimization at the BS

In this subsection, we optimize the covariance matrix \mathbf{R} at the DFRC BS with fixed Φ and $\tilde{\mathbf{t}}$. To handle the requirements of SINR (14b), we can transform the SINR constraint of k -th user into the following form

$$(1 + \Gamma^{-1}) \text{tr}(\mathbf{R}_k \mathbf{H}_k) \geq \text{tr}(\mathbf{R} \mathbf{H}_k) + \sigma_k^2, \forall k, \quad (15)$$

where $\mathbf{H}_k = \mathbf{h}_k \mathbf{h}_k^H$. As a result, Problem (14) can be reformulated as

$$\max_{\mathbf{R}} \min_{l \in \mathcal{L}} \mathbf{a}(\theta_l)^H \Phi \mathbf{H}(\tilde{\mathbf{t}}) \mathbf{R} \mathbf{H}(\tilde{\mathbf{t}})^H \Phi^H \mathbf{a}(\theta_l) \quad (16a)$$

$$\text{s.t.} \quad (1 + \Gamma^{-1}) \text{tr}(\mathbf{R}_k \mathbf{H}_k) \geq \text{tr}(\mathbf{R} \mathbf{H}_k) + \sigma_k^2, \forall k, \quad (16b)$$

$$\text{tr}(\mathbf{R}) \leq P_0, \quad (16c)$$

$$\mathbf{R} \succeq 0, \quad (16d)$$

$$\text{rank}(\mathbf{R}_k) = 1. \quad (16e)$$

Owing to the rank-one constraint (16e), Problem (16) is still non-convex. To handle this problem, we utilize the key idea

of the SDR method. By omitting the rank-one constraints, Problem (16) can be recast as

$$\max_{\mathbf{R}, \{\mathbf{R}_k\}} \min_{l \in \mathcal{L}} \text{tr}(\mathbf{A}(\theta_l)\mathbf{R}) \quad (17a)$$

$$\text{s.t.} \quad (1 + \Gamma^{-1}) \text{tr}(\mathbf{R}_k \mathbf{H}_k) \geq \text{tr}(\mathbf{R} \mathbf{H}_k) + \sigma_k^2, \forall k, \quad (17b)$$

$$\text{tr}(\mathbf{R}) \leq P_0, \quad (17c)$$

$$\mathbf{R} \succeq 0, \quad (17d)$$

$$\mathbf{R} - \sum_{k=1}^K \mathbf{R}_k \succeq 0, \quad (17e)$$

where $\mathbf{A}(\theta_l) = \mathbf{H}^H \Phi^H \mathbf{a}(\theta_l) \mathbf{a}(\theta)^H \Phi \mathbf{H}$ is independent of \mathbf{R} . Problem (17) is a convex SDP problem where all the constraints are either linear or semidefinite and the global optimal point can be obtained in polynomial time by using the convex optimization toolbox CVX [29]. Denoting $\hat{\mathbf{R}}, \{\hat{\mathbf{R}}_k\}$ as a feasible solution to Problem (17), we introduce the following lemma to construct the corresponding rank-one solution $\bar{\mathbf{R}}, \{\bar{\mathbf{R}}_k\}$ to Problem (16).

Lemma: There exists a global optimum $\bar{\mathbf{R}}, \{\bar{\mathbf{R}}_k\}$ for Problem (16), satisfying

$$\text{rank}(\bar{\mathbf{R}}_k) = 1, \forall k. \quad (18)$$

Proof: Please refer to [15]. ■

B. Reflective Beamforming Optimization

In this subsection, we optimize the phase shift Φ of the RIS, with fixed transmit covariance matrix \mathbf{R} and fixed position $\tilde{\mathbf{t}}$ of M MAs. The subproblem can be rewritten as

$$\max_{\Phi} \min_{l \in \mathcal{L}} \mathbf{a}(\theta)^H \Phi \mathbf{H}(\tilde{\mathbf{t}}) \mathbf{R} \mathbf{H}(\tilde{\mathbf{t}})^H \Phi^H \mathbf{a}(\theta_l) \quad (19a)$$

$$\text{s.t.} \quad \text{SINR}_k \geq \Gamma, \forall k, \quad (19b)$$

$$\Phi = \text{diag}(e^{j\phi_1}, \dots, e^{j\phi_N}). \quad (19c)$$

We first define $\mathbf{v} \triangleq \text{vec}(\Phi^*) = [e^{j\phi_1}, \dots, e^{j\phi_N}]^H$ and introduce the following definition

$$\mathbf{H}_l \triangleq \text{diag}(\alpha(\theta_l)^H) \mathbf{H}(\tilde{\mathbf{t}}) \mathbf{R} \mathbf{H}(\tilde{\mathbf{t}})^H \text{diag}(\alpha(\theta_l)), \forall l \in \mathcal{L}. \quad (20)$$

Then the beampattern gain towards angle θ_l is rewritten as

$$\mathcal{P}(\theta_l) = \mathbf{v}^H \mathbf{H}_l \mathbf{v}. \quad (21)$$

Next, by letting $\mathbf{G}_k = \text{diag}(\mathbf{h}_{1,k}^H) \mathbf{H}(\tilde{\mathbf{t}})$, the SINR constraint in (14b) is reformulated as

$$(\mathbf{v}^H \mathbf{G}_k + \mathbf{H}_{2,k}^H) \tilde{\mathbf{R}}_k (\mathbf{G}_k^H \mathbf{v} + \mathbf{H}_{2,k}) \geq \sigma^2, \forall k, \quad (22)$$

where $\tilde{\mathbf{R}}_k = (1 + \Gamma^{-1}) \mathbf{R}_k - \mathbf{R}$. In addition, (22) can be further recast as

$$\bar{\mathbf{v}}^H \mathbf{W}_k \bar{\mathbf{v}} \geq \sigma_k^2, \forall k, \quad (23)$$

with

$$\mathbf{W}_k = \begin{bmatrix} \mathbf{G}_k \tilde{\mathbf{R}}_k \mathbf{G}_k^H & \mathbf{G}_k \tilde{\mathbf{R}}_k \mathbf{H}_{2,k} \\ \mathbf{H}_{2,k}^H \tilde{\mathbf{R}}_k \mathbf{G}_k^H & \mathbf{H}_{2,k}^H \tilde{\mathbf{R}}_k \mathbf{H}_{2,k} \end{bmatrix}, \bar{\mathbf{v}} = \begin{bmatrix} \mathbf{v} \\ 1 \end{bmatrix}. \quad (24)$$

For further manipulations, let us define

$$\bar{\mathbf{H}}_l = \begin{bmatrix} \mathbf{H}_l & \mathbf{0}_{N \times 1} \\ \mathbf{0}_{1 \times N} & 0 \end{bmatrix}, \quad (25)$$

and by substituting (24), (25) into (21), we have $\mathcal{P}(\theta) = \bar{\mathbf{v}}^H \bar{\mathbf{H}}_l \bar{\mathbf{v}}$. Hence, Problem (19) can be recast as

$$\max_{\bar{\mathbf{v}}} \min_{l \in \mathcal{L}} \bar{\mathbf{v}}^H \bar{\mathbf{H}}_l \bar{\mathbf{v}} \quad (26a)$$

$$\text{s.t.} \quad \bar{\mathbf{v}}^H \mathbf{W}_k \bar{\mathbf{v}} \geq \sigma_k^2, \forall k, \quad (26b)$$

$$|\bar{v}_n| = 1, \forall n \in \{1, \dots, N+1\}, \quad (26c)$$

which is still non-convex due to the unit-modulus constraints (26c). To address this issue, we define $\bar{\mathbf{V}} = \bar{\mathbf{v}} \bar{\mathbf{v}}^H$ and Problem (26) is reformulated as

$$\max_{\bar{\mathbf{V}}} \min_{l \in \mathcal{L}} \text{tr}(\bar{\mathbf{H}}_l \bar{\mathbf{V}}) \quad (27a)$$

$$\text{s.t.} \quad \text{tr}(\mathbf{W}_k \bar{\mathbf{V}}) \geq \sigma_k^2, \forall k, \quad (27b)$$

$$\bar{V}_{n,n} = 1, \forall n \in \{1, \dots, N+1\}, \quad (27c)$$

$$\bar{\mathbf{V}} \succeq 0, \quad (27d)$$

$$\text{rank}(\bar{\mathbf{V}}) = 1. \quad (27e)$$

The only non-convex constraint in (27) is the rank-one constraint (27e), which can be typically addressed by using the SDR and Gaussian randomization technique. However, in the case of strict constraints, as in Problem (27), the approximation methods such as Gaussian randomization algorithm cannot guarantee the convergence of the overall algorithm [14]. Therefore, we adopt SRCR to convert (27e) equivalently to [30]

$$\mathbf{u}_{\max}^H(\bar{\mathbf{V}}^{(t)}) \bar{\mathbf{V}} \mathbf{u}_{\max}(\bar{\mathbf{V}}^{(t)}) \geq w^{(t)} \text{Tr}(\bar{\mathbf{V}}), \quad (28)$$

where $\bar{\mathbf{V}}^{(t)}$ is a feasible solution obtained in the t -th iteration, $\mathbf{u}_{\max}(\bar{\mathbf{V}}^{(t)})$ is the eigenvector corresponding to the maximum eigenvalue of $\bar{\mathbf{V}}^{(t)}$, $w^{(t)}$ denotes a relaxation parameter which will gradually approach 1. Finally, our optimization problem in the t -th iteration is given by

$$\max_{\bar{\mathbf{V}}} \min_{l \in \mathcal{L}} \text{tr}(\bar{\mathbf{H}}_l \bar{\mathbf{V}}) \quad (29a)$$

$$\text{s.t.} \quad \text{tr}(\mathbf{W}_k \bar{\mathbf{V}}) \geq \sigma_k^2, \forall k, \quad (29b)$$

$$\bar{V}_{n,n} = 1, \forall n \in \{1, \dots, N+1\}, \quad (29c)$$

$$\bar{\mathbf{V}} \succeq 0, \quad (29d)$$

$$\mathbf{u}_{\max}^H(\bar{\mathbf{V}}^{(t)}) \bar{\mathbf{V}} \mathbf{u}_{\max}(\bar{\mathbf{V}}^{(t)}) \geq w^{(t)} \text{Tr}(\bar{\mathbf{V}}). \quad (29e)$$

Problem (29) is an SDP problem and can be solved by the CVX tool [29]. The procedure for optimizing RIS reflecting coefficients is summarized in Algorithm 1.

C. Antenna Position Design

In this subsection, we optimize the position $\tilde{\mathbf{t}}$ of M MAs, with fixed transmit covariance matrix \mathbf{R} and reflecting coeffi-

Algorithm 1 SRCR Algorithm for Optimizing RIS Coefficients

1: **Input:** $\{\bar{\mathbf{H}}_l\}_{l=1}^L, \{\mathbf{W}_k\}_{k=1}^K$.
 2: Initialize $\{\mathbf{t}_m\}_{m=1}^M, w^{(0)} = 0, \tau^{(0)}$.
 3: **while** $\text{Tr}(\bar{\mathbf{V}}^{(t)}) / \lambda_{\max}(\bar{\mathbf{V}}^{(t)}) - 1$ is above ϵ **do**
 4: **if** Problem (29) is solvable with $\mathbf{V}^{(t)}$ and $w^{(t)}$ **then**
 5: Obtain $\bar{\mathbf{V}}^{(t+1)}$ by solving Problem (29), $\tau^{(t+1)} = \tau^{(0)}$
 6: **else**
 7: Update $\bar{\mathbf{V}}^{(t+1)} = \bar{\mathbf{V}}^{(t)}$;
 8: Update $\tau^{(t+1)} = \tau^{(t)} / 2$;
 9: **end if**
 10: $w^{(t+1)} = \min\left(1, \frac{\lambda_{\max}(\bar{\mathbf{V}}^{(t+1)})}{\text{Tr}(\bar{\mathbf{V}}^{(t+1)})} + \tau^{(t+1)}\right)$;
 11: $t = t + 1$;
 12: **end while**
 13: Obtain Φ by decompose $\bar{\mathbf{V}}$.
 14: **Output:** Φ .

cient Φ . The optimization problem can be further reformulated as

$$\max_{\tilde{\mathbf{t}}} \min_{l \in \mathcal{L}} \mathbf{a}(\theta)^H \Phi \mathbf{H}(\tilde{\mathbf{t}}) \mathbf{R} \mathbf{H}(\tilde{\mathbf{t}})^H \Phi^H \mathbf{a}(\theta_l) \quad (30a)$$

$$\text{s.t. SINR}_k \geq \Gamma, \forall k, \quad (30b)$$

$$\|\mathbf{t}_k - \mathbf{t}_q\|_2 \geq D, k \neq q, \quad (30c)$$

$$\tilde{\mathbf{t}} \in \mathcal{C}, \quad (30d)$$

which is a non-convex problem owing to the complex form of the objective function and the non-convex constraints. To deal with the max-min objective function, we first introduce an auxiliary variable χ , and the problem can be reformulated as

$$\max_{\tilde{\mathbf{t}}} \chi \quad (31a)$$

$$\text{s.t. } \mathbf{a}(\theta)^H \Phi \mathbf{H}(\tilde{\mathbf{t}}) \mathbf{R} \mathbf{H}(\tilde{\mathbf{t}})^H \Phi^H \mathbf{a}(\theta_l) \geq \chi, l \in \mathcal{L}, \quad (31b)$$

$$\text{SINR}_k \geq \Gamma, \forall k, \quad (31c)$$

$$\|\mathbf{t}_k - \mathbf{t}_q\|_2 \geq D, k \neq q, \quad (31d)$$

$$\tilde{\mathbf{t}} \in \mathcal{C}. \quad (31e)$$

The main challenges of solving Problem (31) lie in the complicated expressions of $\mathbf{H}(\tilde{\mathbf{t}})$, $\mathbf{h}_{1,k}(\tilde{\mathbf{t}})$ and the tight coupling of $\{\mathbf{t}_m\}_{m=1}^M$. To this end, we aim to solve Problem (31) in an alternating manner. Specifically, we solve M subproblems of (31), which respectively optimize one transmit MA position \mathbf{t}_m , with all the other variables being fixed. The developed alternating optimization algorithm can obtain a locally sub-optimal solution for Problem (31) by solving the above M subproblems alternately.

We next consider the optimization of \mathbf{t}_m with given $\{\mathbf{t}_q\}_{q \neq m}$. For constraint (31c), we first rewrite the SINR constraint with respect to the k -th user as

$$\mathbf{h}_k^H [(1 + \Gamma^{-1}) \mathbf{R}_k - \mathbf{R}] \mathbf{h}_k \geq \sigma_k^2. \quad (32)$$

Since the antenna position \mathbf{t}_m is only related to $\mathbf{g}(\mathbf{t}_m)$, we can convert constraint (32) to a more tractable form

$$(\mathbf{p}_k^H \mathbf{G}(\tilde{\mathbf{t}}) + \mathbf{q}_k^H \mathbf{G}_k(\tilde{\mathbf{t}})) \tilde{\mathbf{R}}_k (\mathbf{G}(\tilde{\mathbf{t}})^H \mathbf{p}_k + \mathbf{G}_k(\tilde{\mathbf{t}})^H \mathbf{q}_k) \geq \sigma_k^2, \quad (33)$$

where $\mathbf{p}_k^H = \mathbf{h}_{1,k}^H \Phi \mathbf{F}(\mathbf{r})^H \Sigma$ and $\mathbf{q}_k^H = \mathbf{1}^H \Sigma_k$ are invariant to $\tilde{\mathbf{t}}$. We then define $x_{k,q} = \mathbf{p}_k^H \mathbf{g}(\mathbf{t}_q) + \mathbf{q}_k^H \mathbf{g}_k(\mathbf{t}_q), q = 1, 2, \dots, M$, constraint (33) can be recast as

$$\underbrace{\left[\tilde{\mathbf{R}}_k \right]_{m,m} |x_{k,m}|^2 + 2\Re\{\tilde{a}_k x_{k,m}\}}_{\tilde{I}(\mathbf{t}_m)} \geq \sigma_k^2 - \tilde{b}_k, \quad (34)$$

where \tilde{a}_k and \tilde{b}_k are given at the bottom of the next page. It is worth noting that $x_{k,m}$ is the optimization variable related to the antenna position \mathbf{t}_m , while \tilde{a}_k and \tilde{b}_k are variables invariant to \mathbf{t}_m . To fully reveal the optimization variable \mathbf{t}_m in the current form of constraint (34), we expand the left-hand-side of constraint (34) in (37), as shown at the bottom of the next page. In (37), $\mathbf{P}_k \triangleq \mathbf{p}_k \mathbf{p}_k^H$, $\mathbf{Q}_k \triangleq \mathbf{q}_k \mathbf{q}_k^H$.

However, $\tilde{I}(\mathbf{t}_m)$ is neither concave nor convex with respect to \mathbf{t}_m , making constraint (34) still non-convex and thus intractable. To tackle this problem, we use the SCA method and transform the non-convex constraint. Specifically, by using the Taylor's theorem, we can construct a quadratic surrogate function which serves as a strict convex constraint to (34). With given local point $\mathbf{t}_m^{(i)} \in \mathbb{R}^2$ in the i -th iteration, a lower bound can be obtained as $\tilde{I}(\mathbf{t}_m) \geq \tilde{I}(\mathbf{t}_m^{(i)}) + \nabla \tilde{I}(\mathbf{t}_m^{(i)})^T (\mathbf{t}_m - \mathbf{t}_m^{(i)}) - \frac{\tilde{\delta}_m^{(i)}}{2} (\mathbf{t}_m - \mathbf{t}_m^{(i)})^T (\mathbf{t}_m - \mathbf{t}_m^{(i)})$, where $\tilde{\delta}_m^{(i)}$ is a positive real number which satisfies $\tilde{\delta}_m^{(i)} \mathbf{I}_2 \succeq \nabla^2 \tilde{I}(\mathbf{t}_m)$. The gradient vector $\nabla \tilde{I}(\mathbf{t}_m)$ and the Hessian matrix $\nabla^2 \tilde{I}(\mathbf{t}_m)$ are given in Appendix A. According to Appendix A and $\|\nabla^2 \tilde{I}(\mathbf{t}_m)\|_2 \mathbf{I}_2 \succeq \nabla^2 \tilde{I}(\mathbf{t}_m)$, we can construct $\tilde{\delta}_m^{(i)}$ as follows:

$$\begin{aligned} \tilde{\delta}_m^{(i)} &= \frac{64\pi^2}{\lambda} \left[\sum_{i=1}^{L_t^{k-1}} \sum_{j=i+1}^{L_t^k} \left[\tilde{\mathbf{R}}_k \right]_{m,m} |[\mathbf{Q}_k]_{i,j}| \right. \\ &\quad + \sum_{i=1}^{L_t^{k-1}} \sum_{j=i+1}^{L_t^k} \left[\tilde{\mathbf{R}}_k \right]_{m,m} |[\mathbf{P}_k]_{i,j}| \\ &\quad \left. + \sum_{i=1}^{L_t} \sum_{j=1}^{L_t^k} \left[\tilde{\mathbf{R}}_k \right]_{m,m} |[\mathbf{p}_k]_i| |[\mathbf{q}_k]_j| \right] \\ &\quad + \frac{16\pi^2}{\lambda} \left[\sum_{i=1}^{L_t} |\tilde{a}_k| |[\mathbf{p}_k]_i| + \sum_{j=1}^{L_t^k} |\tilde{a}_k| |[\mathbf{q}_k]_j| \right] \\ &\geq \|\nabla^2 \tilde{I}(\mathbf{t}_m)\|_F \stackrel{(a)}{\geq} \|\nabla^2 \tilde{I}(\mathbf{t}_m)\|_2, \end{aligned} \quad (38)$$

which satisfies $\tilde{\delta}_m^{(i)} \mathbf{I}_2 \succeq \|\nabla^2 \tilde{I}(\mathbf{t}_m)\|_2 \mathbf{I}_2 \succeq \nabla^2 \tilde{I}(\mathbf{t}_m)$. The inequality marked by (a) holds because $\|\nabla^2 \tilde{I}(\mathbf{t}_m)\|_F = \sqrt{\sum_{i=1} \sigma_i^2(\nabla^2 \tilde{I}(\mathbf{t}_m))} \geq \sigma_{\max}(\nabla^2 \tilde{I}(\mathbf{t}_m)) = \|\nabla^2 \tilde{I}(\mathbf{t}_m)\|_2$, where $\sigma_i(\nabla^2 \tilde{I}(\mathbf{t}_m))$ are the singular values of $\nabla^2 \tilde{I}(\mathbf{t}_m)$. Thus

we can rewrite constraint (34) as

$$\begin{aligned}
\tilde{I}(\mathbf{t}_m) &\geq \tilde{I}(\mathbf{t}_m^{(i)}) + \nabla \tilde{I}(\mathbf{t}_m^{(i)})^T (\mathbf{t}_m - \mathbf{t}_m^{(i)}) \\
&\quad - \frac{\tilde{\delta}_m^{(i)}}{2} (\mathbf{t}_m - \mathbf{t}_m^{(i)})^T (\mathbf{t}_m - \mathbf{t}_m^{(i)}) \\
&= -\frac{\tilde{\delta}_m^{(i)}}{2} \mathbf{t}_m^T \mathbf{t}_m + \left(\nabla \tilde{I}(\mathbf{t}_m^{(i)}) + \tilde{\delta}_m^{(i)} \mathbf{t}_m^{(i)} \right)^T \mathbf{t}_m \\
&\quad + \underbrace{\tilde{I}(\mathbf{t}_m^{(i)}) - \frac{\tilde{\delta}_m^{(i)}}{2} (\mathbf{t}_m^{(i)})^T \mathbf{t}_m^{(i)} - \nabla \tilde{I}(\mathbf{t}_m^{(i)})^T \mathbf{t}_m^{(i)}}_{\text{const}} \\
&\geq \sigma^2 - \tilde{b}_k. \tag{39}
\end{aligned}$$

Next, we tackle the non-convexity of constraint (31b). Define $\mathbf{d}(\theta_l)^H = \mathbf{a}(\theta_l)^H \Phi \mathbf{F}(\mathbf{r})^H \Sigma$, and constraint (31b) can be rewritten as

$$\begin{aligned}
&\mathbf{a}(\theta_l)^H \Phi \mathbf{H}(\tilde{\mathbf{t}}) \mathbf{R} \mathbf{H}(\tilde{\mathbf{t}})^H \Phi^H \mathbf{a}(\theta_l) \\
&= \underbrace{\mathbf{d}(\theta_l)^H \mathbf{A}(\mathbf{t}_m) \mathbf{d}(\theta_l) + [\mathbf{R}]_{m,m} |\mathbf{d}(\theta_l)^H \mathbf{g}(\mathbf{t}_m)|^2}_{\tilde{I}(\mathbf{t}_m)} \\
&\quad + \mathbf{d}(\theta_l)^H \mathbf{B}_m \mathbf{d}(\theta_l) \geq \chi, \tag{40}
\end{aligned}$$

where $\mathbf{A}(\mathbf{t}_m)$ is a linear function of $\mathbf{g}(\mathbf{t}_m)$ and \mathbf{B}_m is a constant matrix independent of \mathbf{t}_m , which are defined in (41) and (42) respectively at the bottom of the next page. Since $I(\mathbf{t}_m)$ can be lower bounded by its first-order Taylor expansion, we apply the SCA method and the non-convex constraint (40) can be rewritten as

$$\begin{aligned}
&2[\mathbf{R}]_{m,m} \Re \left\{ \mathbf{g}(\mathbf{t}_m^{(i)})^H \mathbf{d}(\theta_l) \mathbf{d}(\theta_l)^H \mathbf{g}(\mathbf{t}_m) \right\} + \underbrace{\mathbf{d}(\theta_l)^H \mathbf{A}(\mathbf{t}_m) \mathbf{d}(\theta_l)}_{\tilde{I}(\mathbf{t}_m)} \\
&\geq \chi - \mathbf{d}(\theta_l)^H \mathbf{B}_m \mathbf{d}(\theta_l) + [\mathbf{R}]_{m,m} \left| \mathbf{d}(\theta_l)^H \mathbf{g}(\mathbf{t}_m^{(i)}) \right|^2. \tag{43}
\end{aligned}$$

Here $\tilde{I}(\mathbf{t}_m)$ is a linear function of $\mathbf{g}(\mathbf{t}_m)$, though it is still neither concave nor convex over \mathbf{t}_m . Analogous to (39), we can construct a second-order Taylor expansion-based concave lower bound for $\tilde{I}(\mathbf{t}_m)$. For ease of exposition, we define $\mathbf{b}_1^T \triangleq 2[\mathbf{R}]_{m,m} \mathbf{g}(\mathbf{t}_m^{(i)})^H \mathbf{d}_l(\theta) \mathbf{d}_l(\theta)^H$, $\mathbf{b}_2^T \triangleq 2 \sum_{q=1, q \neq m}^M ([\mathbf{R}]_{m,q} \mathbf{g}(\mathbf{t}_q)^H) \mathbf{d}(\theta_l) \mathbf{d}(\theta_l)^H$ and $\mathbf{b} = \mathbf{b}_1 + \mathbf{b}_2$. Thus $\tilde{I}(\mathbf{t}_m)$ can be rewritten as

$$\begin{aligned}
\tilde{I}(\mathbf{t}_m) &= \Re \left\{ 2[\mathbf{R}]_{m,m} \mathbf{g}(\mathbf{t}_m^{(i)})^H \mathbf{d}(\theta_l) \mathbf{d}(\theta_l)^H \mathbf{g}(\mathbf{t}_m) \right\} \\
&\quad + \Re \left\{ 2\mathbf{d}(\theta_l)^H \left(\sum_{q=1, q \neq m}^M [\mathbf{R}]_{m,q} \mathbf{g}(\mathbf{t}_q)^H \right) \mathbf{d}(\theta_l) \mathbf{g}(\mathbf{t}_m) \right\} \\
&= \Re \left\{ \mathbf{b}_1^T \mathbf{g}(\mathbf{t}_m) + \mathbf{b}_2^T \mathbf{g}(\mathbf{t}_m) \right\} \\
&= \Re \left\{ \mathbf{b}^T \mathbf{g}(\mathbf{t}_m) \right\} \\
&= \sum_{k=1}^{L_t} |[\mathbf{b}]_k| \cos(\varrho^k(\mathbf{t}_m)), \tag{44}
\end{aligned}$$

where $\varrho^k(\mathbf{t}_m) \triangleq 2\pi \rho_t^k(\mathbf{t}_m) / \lambda + \angle[\mathbf{b}]_k$. In a similar way, we can calculate the the gradient vector $\nabla \tilde{I}(\mathbf{t}_m)$ and the Hessian matrix $\nabla^2 \tilde{I}(\mathbf{t}_m)$ of $\tilde{I}(\mathbf{t}_m)$, which are omitted for simplicity.

$$\tilde{a}_k = \sum_{q=1, q \neq m}^M [\tilde{\mathbf{R}}_k]_{m,q} x_{k,q}^* \tag{35}$$

$$\tilde{b}_k = \sum_{p=1, p \neq m}^M \left(\sum_{q=1, q \neq m}^{p-1} 2\Re\{[\tilde{\mathbf{R}}_k]_{p,q} x_{k,p} x_{k,q}^*\} + [\tilde{\mathbf{R}}_k]_{p,p} |x_{k,p}|^2 \right) \tag{36}$$

$$\begin{aligned}
\tilde{I}(\mathbf{t}_m) &= [\tilde{\mathbf{R}}_k]_{m,m} (\mathbf{g}_k(\mathbf{t}_m)^H \mathbf{Q}_k \mathbf{g}_k(\mathbf{t}_m) + \mathbf{g}(\mathbf{t}_m)^H \mathbf{P}_k \mathbf{g}(\mathbf{t}_m) + 2\Re\{\mathbf{p}_k^H \mathbf{g}(\mathbf{t}_m) \mathbf{g}_k(\mathbf{t}_m)^H \mathbf{q}_k\}) + 2\Re\{\tilde{a}_k \mathbf{p}_k^H \mathbf{g}(\mathbf{t}_m) + \tilde{a}_k \mathbf{q}_k^H \mathbf{g}_k(\mathbf{t}_m)\}) \\
&= 2 \sum_{i=1}^{L_t^k-1} \sum_{j=i+1}^{L_t^k} 2 [\tilde{\mathbf{R}}_k]_{m,m} |[\mathbf{Q}_k]_{i,j}| \cos\left(\frac{2\pi}{\lambda} (\rho_{t,k}^i(\mathbf{t}_m) - \rho_{t,k}^j(\mathbf{t}_m)) + \angle[\mathbf{Q}_k]_{i,j}\right) + \sum_{i=1}^{L_t^k} [\tilde{\mathbf{R}}_k]_{m,m} |[\mathbf{Q}_k]_{i,i}| \\
&\quad + 2 \sum_{i=1}^{L_t-1} \sum_{j=i+1}^{L_t} [\tilde{\mathbf{R}}_k]_{m,m} |[\mathbf{P}_k]_{i,j}| \cos\left(\frac{2\pi}{\lambda} (\rho_t^i(\mathbf{t}_m) - \rho_t^j(\mathbf{t}_m)) + \angle[\mathbf{P}_k]_{i,j}\right) + \sum_{i=1}^{L_t} [\tilde{\mathbf{R}}_k]_{m,m} |[\mathbf{P}_k]_{i,i}| \\
&\quad + 2 \sum_{i=1}^{L_t} \sum_{j=1}^{L_t^k} [\tilde{\mathbf{R}}_k]_{m,m} |[\mathbf{p}_k]_i| |[\mathbf{q}_k]_j| \cos\left(\frac{2\pi}{\lambda} (\rho_t^i(\mathbf{t}_m) - \rho_{t,k}^j(\mathbf{t}_m)) + \angle[\mathbf{q}_k]_j - \angle[\mathbf{p}_k]_i\right) \\
&\quad + 2 \sum_{i=1}^{L_t} |\tilde{a}_k| |[\mathbf{p}_k]_i| \cos\left(\frac{2\pi}{\lambda} \rho_t^i(\mathbf{t}_m) - \angle[\mathbf{p}_k]_i + \angle \tilde{a}_k\right) + 2 \sum_{j=1}^{L_t^k} |\tilde{a}_k| |[\mathbf{q}_k]_j| \cos\left(\frac{2\pi}{\lambda} \rho_{t,k}^j(\mathbf{t}_m) - \angle[\mathbf{q}_k]_j + \angle \tilde{a}_k\right) \tag{37}
\end{aligned}$$

Hence, we can obtain the $\bar{\delta}_m^{(i)}$ as follows:

$$\bar{\delta}_m^{(i)} = \frac{8\pi^2}{\lambda^2} \sum_{k=1}^{L_r} \|\mathbf{b}\|_k, \quad (45)$$

which satisfies $\bar{\delta}_m^{(i)} \mathbf{I}_2 \succeq \|\nabla^2 \bar{I}(\mathbf{t}_m)\|_2 \mathbf{I}_2 \succeq \nabla^2 \bar{I}(\mathbf{t}_m)$. Thus, we can rewrite constraint (43) as

$$\begin{aligned} \bar{I}(\mathbf{t}_m) &\geq \bar{I}(\mathbf{t}_m^{(i)}) + \nabla \bar{I}(\mathbf{t}_m^{(i)})^T (\mathbf{t}_m - \mathbf{t}_m^{(i)}) \\ &\quad - \frac{\delta_n^{(i)}}{2} (\mathbf{t}_m - \mathbf{t}_m^{(i)})^T (\mathbf{t}_m - \mathbf{t}_m^{(i)}) \\ &= -\frac{\delta_n^{(i)}}{2} \mathbf{t}_m^T \mathbf{t}_m + \left(\nabla \bar{I}(\mathbf{t}_m^{(i)}) + \delta_n^{(i)} \mathbf{t}_m^{(i)} \right)^T \mathbf{t}_m \\ &\quad + \underbrace{\bar{I}(\mathbf{t}_m^{(i)}) - \frac{\delta_n^{(i)}}{2} (\mathbf{t}_m^{(i)})^T \mathbf{t}_m^{(i)} - \nabla \bar{I}(\mathbf{t}_m^{(i)})^T \mathbf{t}_m^{(i)}}_{\text{const}} \\ &\geq \chi - \mathbf{d}(\theta_l)^H \mathbf{B}_m \mathbf{d}(\theta_l) + [\mathbf{R}]_{m,m} \left| \mathbf{d}_l(\theta)^H \mathbf{g}(\mathbf{t}_m^{(i)}) \right|^2. \end{aligned} \quad (46)$$

Finally, constraint (31d) can be relaxed at the given point $\mathbf{t}_m^{(i)}$ as follows according to [17]

$$\|\mathbf{t}_m - \mathbf{t}_q\|_2 \geq \frac{1}{\|\mathbf{t}_m^{(i)} - \mathbf{t}_q\|_2} (\mathbf{t}_m^{(i)} - \mathbf{t}_q)^T (\mathbf{t}_m - \mathbf{t}_q) \geq D. \quad (47)$$

Hence, the antenna position design problem can be reformulated as

$$\max_{\mathbf{t}_m} \chi \quad (48a)$$

$$\text{s.t. (31e), (39), (46), (47),} \quad (48b)$$

which is a convex quadratically constrained problem (QCP) that can be solved efficiently by standard convex solvers such as CVX [29].

D. Convergence and Complexity Analysis

Based on the above discussions, the detailed procedure of the overall AO-based algorithm are summarized in Algorithm 2. It is readily verified that the optimal value of Problem (14) monotonically increases in each step of Algorithm 2. Furthermore, the optimal value is upper-bounded. As a result, Algorithm 2 is assured to converge.

Next, we analyze the computational complexity of Algorithm 1. In each iteration, the complexity mainly stems from solving the three subproblems. Firstly, given a solution accuracy ϵ , the worst-case complexity to solve the SDP

Algorithm 2 Alternating Optimization for Solving Problem (14)

- 1: **Input:** $\Sigma, P_0, \sigma, M, N, L_r, L_t, \{\theta_i\}_{i=1}^{L_r}, \{\phi_i^r\}_{i=1}^{L_r}, \{\theta_j^t\}_{j=1}^{L_t}, \{\phi_j^t\}_{j=1}^{L_t}, \mathcal{C}, D, \epsilon_1, \epsilon_2$.
- 2: **Initialize** $\{\mathbf{t}_m\}_{m=1}^M$.
- 3: **while** Increase of the minimum beampattern gain in (13) is above ϵ **do**
- 4: Obtain the optimal solution of \mathbf{R} with given $\tilde{\mathbf{t}}$ and Φ by solving Problem (16).
- 5: Obtain the optimal solution of Φ with given $\tilde{\mathbf{t}}$ and \mathbf{R} by solving Problem (19).
- 6: **for** $n = 1 \rightarrow M$ **do**
- 7: **while** Increase of the minimum beampattern gain in (13) is above ϵ **do**
- 8: Given \mathbf{R}, Φ , solve Problem (48) to update \mathbf{t}_m .
- 9: **end while**
- 10: **end for**
- 11: **end while**
- 12: **Output:** $\mathbf{R}, \Phi, \tilde{\mathbf{t}}$.

Problem (17) is $\mathcal{O}(M^{4.5} \log(1/\epsilon))$ [7]. Let T_1^{\max} and T_2^{\max} denote the maximum number of inner-layer iterations to update Φ and $\tilde{\mathbf{t}}$, respectively. Then, the complexity of updating Φ is given by $\mathcal{O}(T_1^{\max} M^4 \sqrt{N} \log(1/\epsilon))$ [30], and the complexity of updating $\tilde{\mathbf{t}}$ is given by $\mathcal{O}(T_2^{\max} M^{3.5} \log(1/\epsilon))$ [15]. Finally, the total complexity of the overall AO-based algorithm is given by $\mathcal{O}(T_3^{\max} (M^{4.5} + T_1^{\max} M^4 \sqrt{N} + T_2^{\max} M^{3.5}) \log(1/\epsilon))$, where T_3^{\max} is the maximum number of outer-layer iterations of the overall algorithm.

IV. SIMULATION RESULTS

In this section, we present simulation results to assess the performance of the proposed MA and RIS-aided ISAC systems. In the simulation setup, we assume that the BS is fixed at (0, 0) and RIS is located at (12 m, 16 m). The users are randomly distributed in the rectangle area between (20 m, 0) and (40 m, -20 m). We consider the geometry channel model, where the numbers of transmit and receive paths are the same, i.e., $L_t = L_r = L = 4$. According to the aforementioned system model, we consider LoS channel between the BS-RIS link and RIS-User link. In addition, the PRMs of the LoS channels are modeled as $\Sigma[1, 1] \sim \mathcal{CN}(0, K_0 (\frac{d}{d_0})^{-\alpha} \kappa / (\kappa + 1))$ and $\Sigma[p, p] \sim \mathcal{CN}(0, K_0 (\frac{d}{d_0})^{-\alpha} / ((\kappa + 1)(L - 1)))$, $p = 2, 3, \dots, L$, where κ denotes the ratio of the average power for LoS paths to that for NLoS paths. The distance-dependent

$$\mathbf{A}(\mathbf{t}_m) = \sum_{q=1, q \neq m}^M \left([\mathbf{R}]_{m,q} \mathbf{g}(\mathbf{t}_m) \mathbf{g}(\mathbf{t}_q)^H + [\mathbf{R}]_{m,q}^* \mathbf{g}(\mathbf{t}_q) \mathbf{g}(\mathbf{t}_m)^H \right) \quad (41)$$

$$\mathbf{B}_m = \sum_{k=1, k \neq m}^M \left(\sum_{q=1, q \neq m}^{k-1} \left([\mathbf{R}]_{k,q} \mathbf{g}(\mathbf{t}_k) \mathbf{g}(\mathbf{t}_q)^H + [\mathbf{R}]_{k,q}^* \mathbf{g}(\mathbf{t}_q) \mathbf{g}(\mathbf{t}_k)^H \right) + [\mathbf{R}]_{k,k} \mathbf{g}(\mathbf{t}_k) \mathbf{g}(\mathbf{t}_k)^H \right) \quad (42)$$

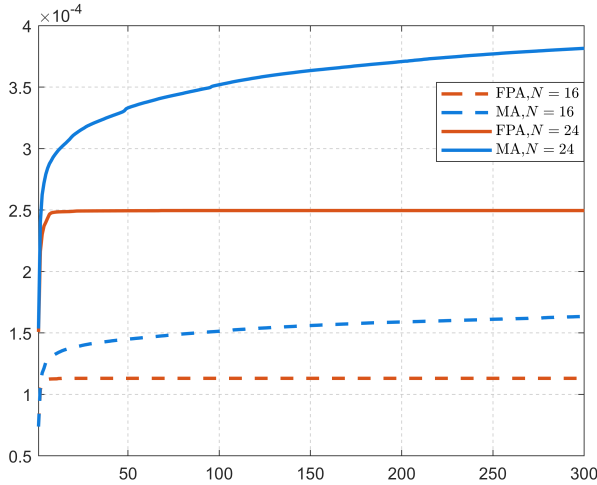


Fig. 3: Convergence behavior.

path-loss is modeled as $K_0(\frac{d}{d_0})^{-\alpha}$, where $K_0 = -40$ dB is the average channel power gain at the reference distance $d_0 = 1$ m and α is the pathloss exponent. Since obstacles exist between the BS-User links, we consider Rayleigh fading and an additional shadow fading with a standard deviation of 15 dB between the NLoS channels. Unless otherwise stated, the simulation parameters are set as follows: The number of MAs at the DFRC BS $M = 8$, the number of downlink users $K = 2$, the interested angles $\{\theta_1, \theta_2, \dots, \theta_5\} = \{-60^\circ, -30^\circ, 0^\circ, 30^\circ, 60^\circ\}$, the transmit power at the DFRC BS $P_0 = 40$ dBm, the user SINR threshold $\Gamma = 10$ dB, the noise power at the receive antenna $\sigma_k^2 = -80$ dBm, the number paths $L = 4$, and the pathloss exponents of BS-RIS, RIS-User, BS-User channels $\alpha = 2.5, 2.5, 3.5$, respectively. All the results are averaged over 400 independent channel realizations.

A. Convergence Behavior of the Proposed Algorithms

The convergence behavior of the proposed algorithm is shown in Fig. 3. As illustrated, the minimum beam pattern gains of all schemes increase with the iteration index and converge within 300 iterations, thus validating the effectiveness of our proposed algorithm. In addition, the MA-aided schemes outperform their FPA-aided counterparts, but require more iterations to converge. This is owing to the procedure of the antenna position optimization in our proposed algorithm.

B. Beam pattern at the RIS

Fig. 4 illustrates the beam pattern gain of the different schemes with $\theta \in [-90^\circ, 90^\circ]$. As depicted in Fig. 4, the values of beam pattern gain in the direction of the interested angles in each scheme are approximately the same, which can be attributed to the principle of fairness inherent in the max-min optimization problem. In addition, the beam pattern gain of the MA-aided schemes exceed their FPA-aided counterpart by approximately 30%, which reveals the advantage of the deployment of MAs at the DFRC BS, owing to its capacity of

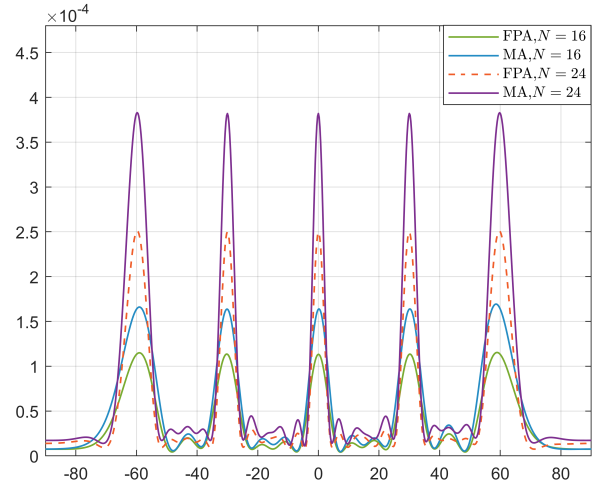


Fig. 4: The beam pattern gains of different schemes.

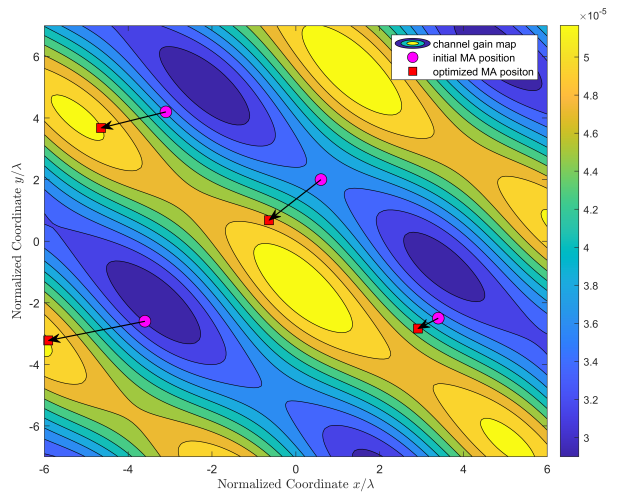


Fig. 5: Example for the channel power gain in the transmit region \mathcal{C} : Movement of $M = 4$ antennas.

channel state configuration and array geometry reconstruction. Furthermore, the increase in the number of the RIS reflecting elements will result in narrower main lobe of the beam pattern, which means better directivity of the sensing function.

C. Channel Characteristics under Antenna Position Optimization

To explore the effect of MA on improving the channel conditions and array geometry, one implementation in which the channel gain of BS-RIS link versus the MAs' positions are presented in Fig. 5. For convenience and clarity, we set the number of antennas as $M = 4$, and the RIS sensing angles $\{\theta_1, \dots, \theta_L\}$ are set to $\{-30^\circ, 0^\circ, 30^\circ\}$ with a service user number $K = 2$, and the channel power gain of the BS-RIS link is defined as $\|\mathbf{H}(\hat{\mathbf{t}})\|^2$. In the implementation, the channel gain $\|\mathbf{H}(\hat{\mathbf{t}})\|^2$ is increased by 12%, which is significantly smaller than the average system performance gain as depicted in Fig.

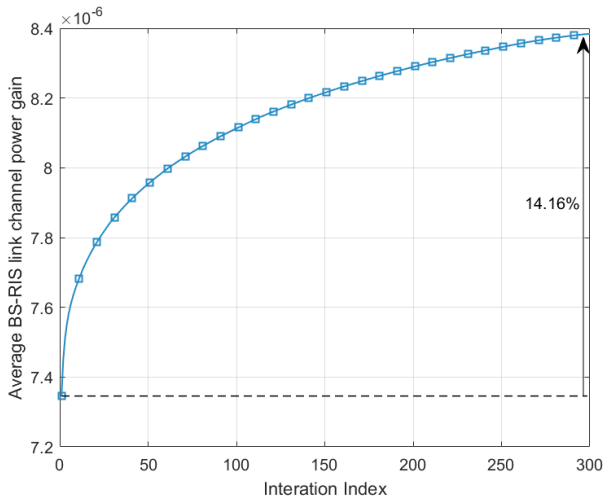


Fig. 6: Channel gain of BS-RIS link versus iteration index

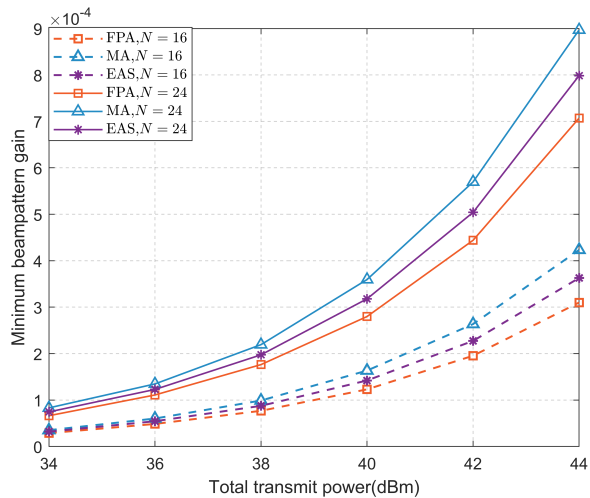


Fig. 8: Minimum beampattern gain versus transmit power P_0 .

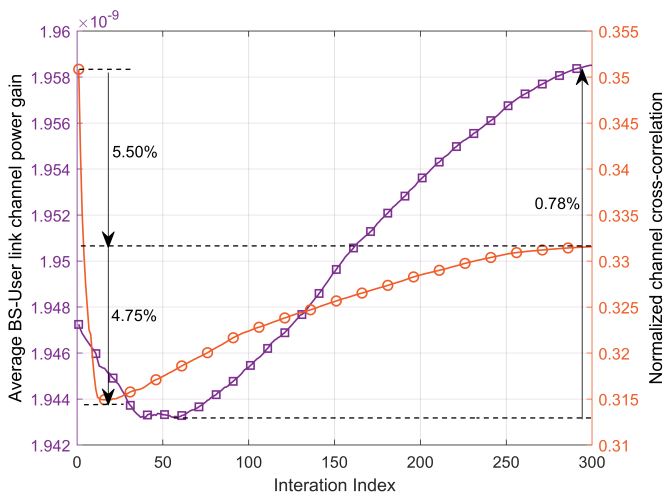


Fig. 7: Average user channel power gain and normalized cross-correlation versus iteration index.

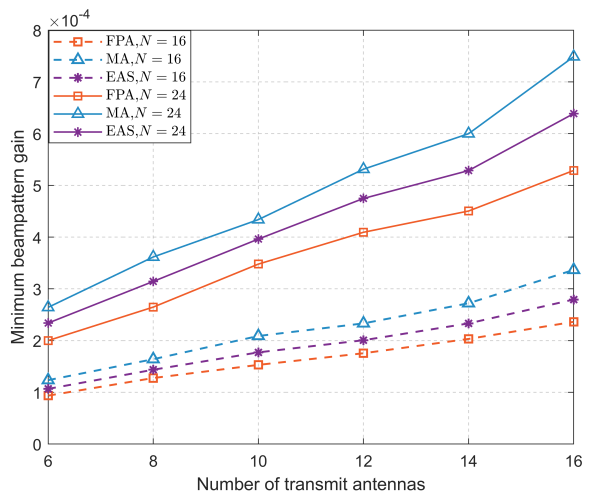


Fig. 9: Minimum beampattern gain versus the number of transmit antennas M .

4. Furthermore, it can be observed that the positions of the MAs are not all optimized to the locations with the maximum channel gain. This is reasonable because the ISAC system needs to simultaneously perform sensing and communication, and the antenna arrays at certain positions can more easily form the desired waveform pattern [27]. In addition, Fig. 6 shows the variation of the average channel gain of the BS-RIS link during the process of antenna position optimization. It can be observed that the channel power gain gradually improves with the number of iterations, once again verifying the role of MA in improving the communication environment by mitigating small-scale fading caused by multipath effects.

Furthermore, we present the average channel gain of user equivalent channel $\|\mathbf{h}_k\|^2$ and cross-correlation coefficient ρ over iteration index in Fig. 7. The cross-correlation coefficient of the equivalent user channels ρ is defined as $\frac{1}{K(K-1)} \sum_{1 \leq k \neq q \leq K} \frac{|\mathbf{h}_k(\mathbf{t})^H \mathbf{h}_q(\mathbf{t})|}{\|\mathbf{h}_k(\mathbf{t})\|_2 \|\mathbf{h}_q(\mathbf{t})\|_2}$. Interestingly, we find that during the procedure of the joint optimization, the varia-

tion of $\|\mathbf{h}_k\|^2$ and ρ can be divided into two phases. In the first phase, the user channel gain decreases by approximately 0.2%, while the user channel similarity decreases by about 10.25%. Therefore, the gain in the ISAC system performance during this phase is partly attributed to the alleviation of multiuser interference, rather than merely enhancing the signal power of individual users. In the second phase, the user channel gain increases by approximately 4.75%, and the channel similarity increases by about 0.78%. This can be attributed to the fact that the channel gain of the BS-RIS link is increasing along with the optimization process to enhance the sensing performance. Moreover, since the channel gain of the BS-RIS link is increasing during the second phase, it is reasonable to expect that both the gain and similarity of the user equivalent channel are also increasing during this phase.

D. Performance Comparison with Benchmark Schemes

To comprehensively illustrate the advantages of MAs in enhancing the sensing and communication performance, we

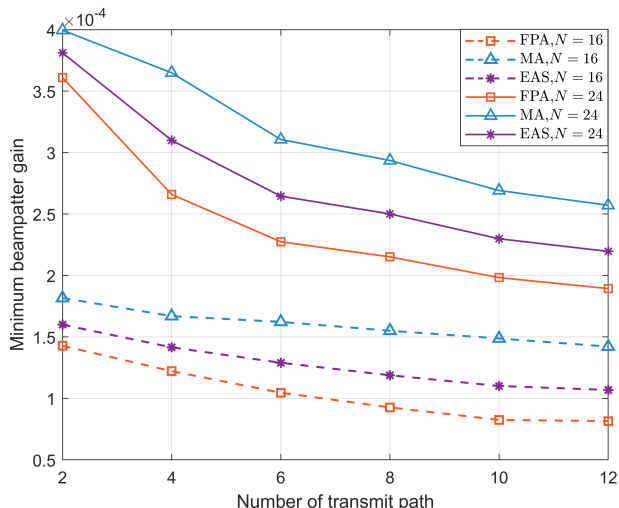


Fig. 10: Minimum beampattern gain versus the number of transmit paths L .

propose the following two baseline schemes:

- 1) **Fixed position antenna (FPA)**: The BS is equipped with a UPA based on FPA configuration, with M antennas spaced between interval of $\frac{\lambda}{2}$.
- 2) **Exhaustive antenna selection (EAS)**: The BS is equipped with an FPA-based UPA, consisting of $2M$ antennas spaced at $\frac{\lambda}{2}$ intervals. From these, M antennas are selected through an exhaustive search.

In Fig. 8, we illustrate the beampattern gain of the proposed and benchmark schemes versus the maximum transmit power P_0 . Firstly, it can be clearly observed that the ISAC system with $N = 24$ RIS elements exhibits approximately a 110% performance improvement over the system with $N = 16$ under three different transmit antenna configurations, demonstrating the importance of deploying RIS in ISAC systems for sensing dead zones. Additionally, the MA scheme, which fully utilizes spatial DoFs, achieves about 30% performance gain over the FPA scheme in all scenarios. This is achieved by simultaneously improving the channel environment, suppressing multi-user interference, and optimizing the geometric characteristics of the antenna array.

Fig. 9 shows the minimum beampattern gain versus the number of transmit antennas. It illustrates that the beampattern gain increases in all schemes due to the spatial diversity gain and array gain introduced by additional antennas. Notably, when the number of antennas doubles from 6 to 12 in the MA-aided scheme with $N = 24$, the beampattern gain increases from 2.73×10^{-4} to 5.34×10^{-4} , achieving a gain of 95.6%. This indicates that increasing the number of MAs can significantly enhance the sensing performance by leveraging the spatial DoFs.

The relationship between the minimum beampattern gain and the number of transmit paths is demonstrated in Fig. 10. It is worth noting that the sensing performance of MA-aided DFRC systems declines with the increase in L , which is contrary to the property that channel capacity tends to increase with the number of transmit paths [17]. This phenomenon can

be attributed to the negative impact of electromagnetic wave scattering on sensing capabilities.

V. CONCLUSION

In this paper, we investigated an MA and RIS-aided ISAC system, where the DFRC BS is equipped with MAs to enhance both sensing and communication performance. Aiming at maximizing the minimum beampattern gain at the RIS towards the desired sensing angles, we jointly optimized the transmit beamforming at the BS, the phase shifts of the RIS and the positions of the MAs, subject to the user SINR constraint and the transmit power constraint at the BS. Due to the highly non-convex nature of the resultant problem, we developed an AO-based algorithm utilizing SDR, SRCR, and SCA techniques. Specifically, the SRCR algorithm was utilized for optimizing the phase shifts at the RIS, owing to the potential nonconvergence characteristics caused by SDR. Simulation results illustrated significant advantages of the MA and RIS-aided system over other baseline schemes in ISAC systems. In addition, this paper meticulously discussed the variation in channel characteristics during the procedure of antenna position optimization. It is observed that the energy of the user channels initially decreases before increasing during the optimization process of the iterative algorithm, which is owing to the deployment of the RIS.

APPENDIX A

The relative terms of gradient vector $\nabla \tilde{I}(\mathbf{t}_m) = \left[\frac{\partial \tilde{I}(\mathbf{t}_m)}{\partial x_m}, \frac{\partial \tilde{I}(\mathbf{t}_m)}{\partial y_m} \right]^T$ are given in (49), (50). For convenience of expression, we define

$$v_{k,i,j}^1(\mathbf{t}_m) = \frac{2\pi}{\lambda} \left(\rho_{t,k}^i(\mathbf{t}_m) - \rho_{t,k}^j(\mathbf{t}_m) \right) + \angle [\mathbf{Q}_k]_{i,j}, \quad (51)$$

$$v_{k,i,j}^2(\mathbf{t}_m) = \frac{2\pi}{\lambda} \left(\rho_t^i(\mathbf{t}_m) - \rho_t^j(\mathbf{t}_m) \right) + \angle [\mathbf{P}_k]_{i,j}, \quad (52)$$

$$v_{k,i,j}^3(\mathbf{t}_m) = \frac{2\pi}{\lambda} \left(\rho_t^i(\mathbf{t}_m) - \rho_{t,k}^j(\mathbf{t}_m) \right) + \angle [\mathbf{q}_k]_j - \angle [\mathbf{p}_k]_i, \quad (53)$$

$$\kappa_{k,i}^1(\mathbf{t}_m) = \frac{2\pi}{\lambda} \rho_t^i(\mathbf{t}_m) - \angle [\mathbf{p}_k]_i + \angle \tilde{a}_k, \quad (54)$$

$$\kappa_{k,j}^2(\mathbf{t}_m) = \frac{2\pi}{\lambda} \rho_{t,k}^i(\mathbf{t}_m) - \angle [\mathbf{q}_k]_j + \angle \tilde{a}_k, \quad (55)$$

and relative terms of the Hessian matrix

$$\nabla^2 \tilde{I}(\mathbf{t}_m) = \begin{bmatrix} \frac{\partial^2 \tilde{I}(\mathbf{t}_m)}{\partial x_m \partial x_m} & \frac{\partial^2 \tilde{I}(\mathbf{t}_m)}{\partial x_m \partial y_m} \\ \frac{\partial^2 \tilde{I}(\mathbf{t}_m)}{\partial y_m \partial x_m} & \frac{\partial^2 \tilde{I}(\mathbf{t}_m)}{\partial y_m \partial y_m} \end{bmatrix} \text{ are given in (56)-}$$

(58). Specifically, $\frac{\partial^2 \tilde{I}(\mathbf{t}_m)}{\partial y_m \partial x_m} = \frac{\partial^2 \tilde{I}(\mathbf{t}_m)}{\partial x_m \partial y_m}$, thus $\frac{\partial^2 \tilde{I}(\mathbf{t}_m)}{\partial y_m \partial x_m}$ is omitted for simplicity.

REFERENCES

- [1] F. Liu, L. Zhou, C. Masouros, A. Li, W. Luo, and A. Petropulu, "Toward dual-functional radar-communication systems: Optimal waveform design," *IEEE Trans. Signal Process.*, vol. 66, pp. 4264–4279, Aug. 2018.
- [2] F. Liu, Y. Cui, C. Masouros, J. Xu, T. X. Han, Y. C. Eldar, and S. Buzzi, "Integrated sensing and communications: Toward dual-functional wireless networks for 6G and beyond," *IEEE J. Sel. Areas Commun.*, vol. 40, pp. 1728–1767, Jun. 2022.

$$\begin{aligned}
\frac{\partial \tilde{I}(\mathbf{t}_m)}{\partial x_m} = & -\frac{4\pi}{\lambda} \sum_{i=1}^{L_t^k-1} \sum_{j=i+1}^{L_t^k} [\tilde{\mathbf{R}}_k]_{m,m} |[\mathbf{Q}_k]_{i,j}| \left(-\cos \phi_{k,i}^t \sin \theta_{k,i}^t + \cos \phi_{k,j}^t \sin \theta_{k,j}^t \right) \sin \left(\frac{2\pi}{\lambda} \left(\rho_{t,k}^i(\mathbf{t}_m) - \rho_{t,k}^j(\mathbf{t}_m) \right) + \angle[\mathbf{Q}_k]_{i,j} \right) \\
& -\frac{4\pi}{\lambda} \sum_{i=1}^{L_t-1} \sum_{j=i+1}^{L_t} [\tilde{\mathbf{R}}_k]_{m,m} |[\mathbf{P}_k]_{i,j}| \left(-\cos \phi_i^t \sin \theta_i^t + \cos \phi_j^t \sin \theta_j^t \right) \sin \left(\frac{2\pi}{\lambda} \left(\rho_t^i(\mathbf{t}_m) - \rho_t^j(\mathbf{t}_m) \right) + \angle[\mathbf{P}_k]_{i,j} \right) \\
& -\frac{4\pi}{\lambda} \sum_{i=1}^{L_t} \sum_{j=1}^{L_t^k} [\tilde{\mathbf{R}}_k]_{m,m} |[\mathbf{p}_k]_i| |[\mathbf{q}_k]_j| \left(-\cos \phi_{k,i}^t \sin \theta_{k,i}^t + \cos \phi_j^t \sin \theta_j^t \right) \sin \left(\frac{2\pi}{\lambda} \left(\rho_{t,k}^i(\mathbf{t}_m) - \rho_{t,k}^j(\mathbf{t}_m) \right) + \angle[\mathbf{q}_k]_j - \angle[\mathbf{p}_k]_i \right) \\
& -\frac{4\pi}{\lambda} \sum_{i=1}^{L_t} |\tilde{a}_k| |[\mathbf{p}_k]_i| \cos \phi_i^t \sin \theta_i^t \sin \left(\frac{2\pi}{\lambda} \rho_t^i(\mathbf{t}_m) - \angle[\mathbf{p}_k]_i + \angle \tilde{a}_k \right) \\
& -\frac{4\pi}{\lambda} \sum_{j=1}^{L_t^k} |\tilde{a}_k| |[\mathbf{q}_k]_j| \cos \phi_{k,j}^t \sin \theta_{k,j}^t \sin \left(\frac{2\pi}{\lambda} \rho_{t,k}^i(\mathbf{t}_m) - \angle[\mathbf{q}_k]_j + \angle \tilde{a}_k \right)
\end{aligned} \tag{49}$$

$$\begin{aligned}
\frac{\partial \tilde{I}(\mathbf{t}_m)}{\partial y_m} = & -\frac{4\pi}{\lambda} \sum_{i=1}^{L_t^k-1} \sum_{j=i+1}^{L_t^k} [\tilde{\mathbf{R}}_k]_{m,m} |[\mathbf{Q}_k]_{i,j}| \left(-\cos \theta_{k,i}^t + \cos \theta_{k,j}^t \right) \sin \left(\frac{2\pi}{\lambda} \left(\rho_{t,k}^i(\mathbf{t}_m) - \rho_{t,k}^j(\mathbf{t}_m) \right) + \angle[\mathbf{Q}_k]_{i,j} \right) \\
& -\frac{4\pi}{\lambda} \sum_{i=1}^{L_t-1} \sum_{j=i+1}^{L_t} [\tilde{\mathbf{R}}_k]_{m,m} |[\mathbf{P}_k]_{i,j}| \left(-\cos \theta_i^t + \cos \theta_j^t \right) \sin \left(\frac{2\pi}{\lambda} \left(\rho_t^i(\mathbf{t}_m) - \rho_t^j(\mathbf{t}_m) \right) + \angle[\mathbf{P}_k]_{i,j} \right) \\
& -\frac{4\pi}{\lambda} \sum_{i=1}^{L_t} \sum_{j=1}^{L_t^k} [\tilde{\mathbf{R}}_k]_{m,m} |[\mathbf{p}_k]_i| |[\mathbf{q}_k]_j| \left(-\cos \theta_{k,i}^t + \cos \theta_j^t \right) \sin \left(\frac{2\pi}{\lambda} \left(\rho_t^i(\mathbf{t}_m) - \rho_{t,k}^j(\mathbf{t}_m) \right) + \angle[\mathbf{q}_k]_j - \angle[\mathbf{p}_k]_i \right) \\
& -\frac{4\pi}{\lambda} \sum_{i=1}^{L_t} |\tilde{a}_k| |[\mathbf{p}_k]_i| \cos \theta_i^t \sin \left(\frac{2\pi}{\lambda} \rho_t^i(\mathbf{t}_m) - \angle[\mathbf{p}_k]_i + \angle \tilde{a}_k \right) \\
& -\frac{4\pi}{\lambda} \sum_{j=1}^{L_t^k} |\tilde{a}_k| |[\mathbf{q}_k]_j| \cos \theta_{k,j}^t \sin \left(\frac{2\pi}{\lambda} \rho_{t,k}^i(\mathbf{t}_m) - \angle[\mathbf{q}_k]_j + \angle \tilde{a}_k \right)
\end{aligned} \tag{50}$$

- [3] I. F. Akyildiz, C. Han, Z. Hu, S. Nie, and J. M. Jornet, "Terahertz band communication: An old problem revisited and research directions for the next decade," *IEEE Trans. Commun.*, vol. 70, pp. 4250–4285, May 2022.
- [4] A. Faisal, H. Sarieddeen, H. Dahrouj, T. Y. Al-Naffouri, and M.-S. Alouini, "Ultramassive MIMO systems at terahertz bands: Prospects and challenges," *IEEE Veh. Technol. Mag.*, vol. 15, pp. 33–42, Oct. 2020.
- [5] A. Hassanien, M. G. Amin, E. Aboutanios, and B. Himed, "Dual-function radar communication systems: A solution to the spectrum congestion problem," *IEEE Veh. Technol. Mag.*, vol. 36, pp. 115–126, Apr. 2019.
- [6] L. Zheng, M. Lops, Y. C. Eldar, and X. Wang, "Radar and communication coexistence: An overview: A review of recent methods," *IEEE Signal Process. Mag.*, vol. 36, pp. 85–99, Sep. 2019.
- [7] X. Liu, T. Huang, N. Shlezinger, Y. Liu, J. Zhou, and Y. C. Eldar, "Joint transmit beamforming for multiuser MIMO communications and MIMO radar," *IEEE Trans. Signal Process.*, vol. 68, pp. 3929–3944, Jun. 2020.
- [8] H. Hua, J. Xu, and T. X. Han, "Optimal transmit beamforming for integrated sensing and communication," *IEEE Trans. Veh. Technol.*, vol. 72, pp. 10588–10603, Aug. 2023.
- [9] J. Zhang, E. Björnson, M. Matthaiou, D. W. K. Ng, H. Yang, and D. J. Love, "Prospective multiple antenna technologies for beyond 5G," *IEEE J. Sel. Areas Commun.*, vol. 38, pp. 1637–1660, Jun. 2020.
- [10] C. Pan, H. Ren, K. Wang, J. F. Kolb, M. El-kashlan, M. Chen, M. Di Renzo, Y. Hao, J. Wang, A. L. Swindlehurst, *et al.*, "Reconfigurable intelligent surfaces for 6G systems: Principles, applications, and research directions," *IEEE Commun. Mag.*, vol. 59, pp. 14–20, Jun. 2021.
- [11] C. Pan, G. Zhou, K. Zhi, S. Hong, T. Wu, Y. Pan, H. Ren, M. Di Renzo, A. L. Swindlehurst, R. Zhang, *et al.*, "An overview of signal processing techniques for RIS/IRS-aided wireless systems," *IEEE J. Sel. Top. Signal Process.*, vol. 16, pp. 883–917, Aug. 2022.
- [12] X. Song, D. Zhao, H. Hua, T. X. Han, X. Yang, and J. Xu, "Joint transmit and reflective beamforming for IRS-assisted integrated sensing and communication," in *IEEE Wireless Commun. Networking Conf. WCNC*, pp. 189–194, IEEE, May 2022.
- [13] R. P. Sankar, S. P. Chepuri, and Y. C. Eldar, "Beamforming in integrated sensing and communication systems with reconfigurable intelligent surfaces," *IEEE Trans. Wireless Commun.*, vol. 23, pp. 4017–4031, Sep. 2024.
- [14] X. Wang, Z. Fei, Z. Zheng, and J. Guo, "Joint waveform design and passive beamforming for RIS-assisted Dual-Functional Radar-Communication system," *IEEE Trans. Veh. Technol.*, vol. 70, pp. 5131–5136, Apr. 2021.
- [15] Z. Yu, H. Ren, C. Pan, G. Zhou, B. Wang, M. Dong, and J. Wang, "Active RIS-aided ISAC systems: Beamforming design and performance analysis," *IEEE Trans. Commun.*, vol. 72, pp. 1578–1595, Nov. 2023.
- [16] K.-K. Wong, A. Shojaeifard, K.-F. Tong, and Y. Zhang, "Fluid antenna systems," *IEEE Trans. Wireless Commun.*, vol. 20, March 2021.
- [17] W. Ma, L. Zhu, and R. Zhang, "MIMO capacity characterization for movable antenna systems," *IEEE Trans. Wireless Commun.*, vol. 23, pp. 3392–3407, Apr. 2024.
- [18] L. Zhu, W. Ma, and R. Zhang, "Modeling and performance analysis for movable antenna enabled wireless communications," *IEEE Trans. Wireless Commun.*, vol. 23, pp. 6234–6250, Jun. 2024.
- [19] W. Ma, L. Zhu, and R. Zhang, "Compressed sensing based channel estimation for movable antenna communications," *IEEE Commun. Lett.*, vol. 27, pp. 2747–2751, Oct. 2023.
- [20] H. Zhang, J. Wang, C. Wang, C.-C. Wang, K.-K. Wong, B. Wang, and C.-B. Chae, "Learning-induced channel extrapolation for fluid antenna

systems using asymmetric graph masked autoencoder,” *IEEE Commun. Lett.*, vol. 13, pp. 1665–1669, Jun. 2024.

- [21] L. Zhu, W. Ma, B. Ning, and R. Zhang, “Movable-antenna enhanced multiuser communication via antenna position optimization,” *IEEE Trans. Wireless Commun.*, pp. 1–1, Dec. 2023.
- [22] G. Hu, Q. Wu, K. Xu, J. Si, and N. Al-Dhahir, “Secure wireless communication via movable-antenna array,” *IEEE Signal Process. Lett.*, vol. 31, pp. 516–520, Jan. 2024.
- [23] J. Tang, C. Pan, Y. Zhang, H. Ren, and K. Wang, “Secure MIMO communication relying on movable antennas,” *arXiv preprint arXiv:2403.04269*, Jan. 2024.
- [24] G. Hu, Q. Wu, K. Xu, J. Ouyang, J. Si, Y. Cai, and N. Al-Dhahir, “Fluid Antennas-Enabled Multiuser Uplink: A Low-Complexity Gradient Descent for Total Transmit Power Minimization,” *IEEE Commun. Lett.*, vol. 28, pp. 602–606, Mar. 2024.
- [25] J. Zheng, T. Wu, X. Lai, C. Pan, M. ElKashlan, and K.-K. Wong, “FAS-assisted NOMA short-packet communication systems,” *IEEE Trans. Veh. Technol.*, pp. 1–6, Feb. 2024.
- [26] W. Ma, L. Zhu, and R. Zhang, “Multi-beam forming with movable-antenna array,” *IEEE Commun. Lett.*, vol. 28, pp. 697–701, Mar. 2024.
- [27] W. Ma, L. Zhu, and R. Zhang, “Movable Antenna Enhanced Wireless Sensing Via Antenna Position Optimization,” *arXiv preprint arXiv:2405.01215*, 2024.
- [28] W. Lyu, S. Yang, Y. Xiu, Z. Zhang, C. Assi, and C. Yuen, “Flexible Beamforming for Movable Antenna-Enabled Integrated Sensing and Communication,” *arXiv preprint arXiv:2405.10507*, 2024.
- [29] S. P. Boyd and L. Vandenberghe, *Convex optimization*. Cambridge university press, 2004.
- [30] J. Zuo, Y. Liu, C. Zhu, Y. Zou, D. Zhang, and N. Al-Dhahir, “Exploiting NOMA and RIS in Integrated Sensing and Communication,” *IEEE Trans. Veh. Technol.*, vol. 72, pp. 12941–12955, May 2023.

$$\begin{aligned}
\frac{\partial^2 \tilde{I}(\mathbf{t}_m)}{\partial y_m \partial y_m} = & -\frac{8\pi^2}{\lambda} \sum_{i=1}^{L_t^k-1} \sum_{j=i+1}^{L_t^k} [\tilde{\mathbf{R}}_k]_{m,m} |[\mathbf{Q}_k]_{i,j}| (-\cos \theta_{k,i}^t + \cos \theta_{k,j}^t)^2 \cos(\iota_{k,i,j}^1(\mathbf{t}_m)) \\
& -\frac{8\pi^2}{\lambda} \sum_{i=1}^{L_t-1} \sum_{j=i+1}^{L_t} [\tilde{\mathbf{R}}_k]_{m,m} |[\mathbf{P}_k]_{i,j}| (-\cos \theta_i^t + \cos \theta_j^t)^2 \cos(\iota_{k,i,j}^2(\mathbf{t}_m)) \\
& -\frac{8\pi^2}{\lambda} \sum_{i=1}^{L_t} \sum_{j=1}^{L_t^k} [\tilde{\mathbf{R}}_k]_{m,m} |[\mathbf{p}_k]_i| |[\mathbf{q}_k]_j| (-\cos \theta_{k,i}^t + \cos \theta_j^t)^2 \cos(\iota_{k,i,j}^3(\mathbf{t}_m)) \\
& -\frac{8\pi^2}{\lambda} \sum_{i=1}^{L_t} |\tilde{a}_k| |[\mathbf{p}_k]_i| \cos^2 \theta_i^t \cos(\kappa_{k,i}^1(\mathbf{t}_m)) - \frac{8\pi^2}{\lambda} \sum_{j=1}^{L_t^k} |\tilde{a}_k| |[\mathbf{q}_k]_j| \cos^2 \theta_{k,j}^t \cos(\kappa_{k,j}^2(\mathbf{t}_m))
\end{aligned} \tag{56}$$

$$\begin{aligned}
\frac{\partial^2 \tilde{I}(\mathbf{t}_m)}{\partial x_m \partial x_m} = & -\frac{8\pi^2}{\lambda} \sum_{i=1}^{L_t^k-1} \sum_{j=i+1}^{L_t^k} [\tilde{\mathbf{R}}_k]_{m,m} |[\mathbf{Q}_k]_{i,j}| (-\cos \phi_{k,i}^t \sin \theta_{k,i}^t + \cos \phi_{k,j}^t \sin \theta_{k,j}^t)^2 \cos(\iota_{k,i,j}^1(\mathbf{t}_m)) \\
& -\frac{8\pi^2}{\lambda} \sum_{i=1}^{L_t-1} \sum_{j=i+1}^{L_t} [\tilde{\mathbf{R}}_k]_{m,m} |[\mathbf{P}_k]_{i,j}| (-\cos \phi_i^t \sin \theta_i^t + \cos \phi_j^t \sin \theta_j^t)^2 \cos(\iota_{k,i,j}^2(\mathbf{t}_m)) \\
& -\frac{8\pi^2}{\lambda} \sum_{i=1}^{L_t} \sum_{j=1}^{L_t^k} [\tilde{\mathbf{R}}_k]_{m,m} |[\mathbf{p}_k]_i| |[\mathbf{q}_k]_j| (-\cos \phi_{k,i}^t \sin \theta_{k,i}^t + \cos \phi_j^t \sin \theta_j^t)^2 \cos(\iota_{k,i,j}^3(\mathbf{t}_m)) \\
& -\frac{8\pi^2}{\lambda} \sum_{i=1}^{L_t} |\tilde{a}_k| |[\mathbf{p}_k]_i| \cos^2 \phi_i^t \sin^2 \theta_i^t \cos(\kappa_{k,i}^1(\mathbf{t}_m)) - \frac{8\pi^2}{\lambda} \sum_{j=1}^{L_t^k} |\tilde{a}_k| |[\mathbf{q}_k]_j| \cos^2 \phi_{k,j}^t \sin^2 \theta_{k,j}^t \cos(\kappa_{k,j}^2(\mathbf{t}_m))
\end{aligned} \tag{57}$$

$$\begin{aligned}
\frac{\partial^2 \tilde{I}(\mathbf{t}_m)}{\partial x_m \partial y_m} = & -\frac{8\pi^2}{\lambda} \sum_{i=1}^{L_t^k-1} \sum_{j=i+1}^{L_t^k} [\tilde{\mathbf{R}}_k]_{m,m} |[\mathbf{Q}_k]_{i,j}| (-\cos \phi_{k,i}^t \sin \theta_{k,i}^t + \cos \phi_{k,j}^t \sin \theta_{k,j}^t) (-\cos \theta_{k,i}^t + \cos \theta_{k,j}^t) \cos(\iota_{k,i,j}^1(\mathbf{t}_m)) \\
& -\frac{8\pi^2}{\lambda} \sum_{i=1}^{L_t-1} \sum_{j=i+1}^{L_t} [\tilde{\mathbf{R}}_k]_{m,m} |[\mathbf{P}_k]_{i,j}| (-\cos \phi_i^t \sin \theta_i^t + \cos \phi_j^t \sin \theta_j^t) (-\cos \theta_i^t + \cos \theta_j^t) \cos(\iota_{k,i,j}^2(\mathbf{t}_m)) \\
& -\frac{8\pi^2}{\lambda} \sum_{i=1}^{L_t} \sum_{j=1}^{L_t^k} [\tilde{\mathbf{R}}_k]_{m,m} |[\mathbf{p}_k]_i| |[\mathbf{q}_k]_j| (-\cos \phi_{k,i}^t \sin \theta_{k,i}^t + \cos \phi_j^t \sin \theta_j^t) (-\cos \theta_{k,i}^t + \cos \theta_j^t) \cos(\iota_{k,i,j}^3(\mathbf{t}_m)) \\
& -\frac{8\pi^2}{\lambda} \sum_{i=1}^{L_t} |\tilde{a}_k| |[\mathbf{p}_k]_i| \cos \phi_i^t \sin \theta_i^t \cos \theta_i^t \cos(\kappa_{k,i}^1(\mathbf{t}_m)) - \frac{8\pi^2}{\lambda} \sum_{j=1}^{L_t^k} |\tilde{a}_k| |[\mathbf{q}_k]_j| \cos \phi_{k,j}^t \sin \theta_{k,j}^t \cos \theta_{k,j}^t \cos(\kappa_{k,j}^2(\mathbf{t}_m))
\end{aligned} \tag{58}$$